

Multiple pathways for ultrafast transduction of light energy in the photosynthetic reaction center of *Rhodobacter sphaeroides*

MARION E. VAN BREDERODE[†], FRANK VAN MOURIK[†], IVO H. M. VAN STOKKUM[†], MICHAEL R. JONES[‡],
AND RIENK VAN GRONDELLE^{†§}

[†]Faculty of Sciences, Vrije Universiteit, de Boelelaan 1081, 1081 HV Amsterdam, The Netherlands; and [‡]Department of Molecular Biology and Biotechnology, University of Sheffield, Western Bank, Sheffield, S10 2UH, United Kingdom

Edited by Robin M. Hochstrasser, University of Pennsylvania, Philadelphia, PA, and approved December 21, 1998 (received for review July 8, 1998)

ABSTRACT A pathway of electron transfer is described that operates in the wild-type reaction center (RC) of the photosynthetic bacterium *Rhodobacter sphaeroides*. The pathway does not involve the excited state of the special pair dimer of bacteriochlorophylls (P^{*}), but instead is driven by the excited state of the monomeric bacteriochlorophyll (B_A^{*}) present in the active branch of pigments along which electron transfer occurs. Pump-probe experiments were performed at 77 K on membrane-bound RCs by using different excitation wavelengths, to investigate the formation of the charge separated state P⁺H_A⁻. In experiments in which P or B_A was selectively excited at 880 nm or 796 nm, respectively, the formation of P⁺H_A⁻ was associated with similar time constants of 1.5 ps and 1.7 ps. However, the spectral changes associated with the two time constants are very different. Global analysis of the transient spectra shows that a mixture of P⁺B_A⁻ and P^{*} is formed in parallel from B_A^{*} on a subpicosecond time scale. In contrast, excitation of the inactive branch monomeric bacteriochlorophyll (B_B) and the high exciton component of P (P₋) resulted in electron transfer only after relaxation to P^{*}. The multiple pathways for primary electron transfer in the bacterial RC are discussed with regard to the mechanism of charge separation in the RC of photosystem II from higher plants.

The success of photosynthesis, in which the energy of a photon is converted into a transmembrane electrochemical potential difference, is determined by the efficiency of charge separation across an energy-transducing membrane occurring inside photosynthetic reaction centers (RCs). In purple bacteria such as *Rhodobacter sphaeroides*, the bacteriochlorophyll (Bchl), bacteriopheophytin (Bphe), and quinone cofactors of the RC are arranged in two near-symmetrical branches that span the membrane (1, 2), but electron transfer proceeds only along the active or A branch, (reviewed in ref. 3). Charge separation is driven by the lowest excited state of a special pair of Bchls (termed primary donor, or P) located close to the periplasmic face of the RC. At room temperature the P^{*} excited state evolves in 3–5 ps into a state in which P is oxidized and a Bphe located halfway across the membrane (H_A) is reduced (3, 4). At 77 K, formation of this P⁺H_A⁻ state occurs in 1–2 ps (5, 6). It now is becoming accepted that electron transfer from P^{*} to P⁺H_A⁻ proceeds via the anion of the accessory Bchl, B_A, located between P and H_A. At room temperature P⁺B_A⁻ is formed as a short-lived, intermediate with a lifetime of 0.9–1.5 ps (7–11). Charge separation is completed by electron transfer from P⁺H_A⁻ to P⁺Q_A⁻ in approximately 200 ps at room temperature and 80 ps at 77 K (3).

Until recently it generally was accepted that excitation of the RC bacteriopheophytins or monomeric Bchls resulted in

downhill energy transfer to P within a few hundreds of femtoseconds, forming P^{*} that drives charge separation (12–15). However, steady-state fluorescence excitation experiments conducted at 77 K on mutant RCs in which P^{*} has a very long lifetime have shown that, despite their rapidity, the efficiency of this energy transfer is not 100% (16, 17). In particular, it was shown that most of the excitation energy residing on B_A and H_A was not transferred to P, but that nevertheless B_A^{*} and H_A^{*} were efficient in the formation of the charge separated state P⁺Q_A⁻ (16). This finding implied that an ultrafast and efficient alternative pathway for charge separation driven by monomeric pigments must exist. For the YM210W and YM210L mutants, in which the rate of P^{*}-driven charge separation is slowed down to hundreds of ps, the presence of this alternative pathway for primary charge separation could be clearly resolved in pump-probe experiments (17, 18). The charge-separated states formed from B_A^{*} in 200 fs were interpreted as P⁺B_A⁻ and B_A⁺H_A⁻, which in turn evolved to P⁺H_A⁻ in a few ps. In addition, excitation of B_A led to some energy transfer from B_A^{*} to P. However, because of the much slower decay of P^{*}, charge separation driven by B_A^{*} and P^{*} was very well separated in time.

The purpose of the experiments described in this paper is to clarify whether the alternative processes, that are clearly resolved in experiments with mutant RCs such as YM210W, also operate in the wild-type (WT) RC. Recent pump-probe experiments on RCs of *R. sphaeroides* strain R-26 showed an excitation wavelength dependence of the absorbance difference spectra that persisted at delay times after which subpicosecond energy transfer was complete (19–21). This finding is an indication that alternative charge separation processes do operate in the WT RC. However, the complicating factor in trying to detect an ultrafast alternative pathway for charge separation in the WT RC is that P^{*}-driven charge separation is also ultrafast, and so the combined characteristics of energy transfer, electron transfer, and possible other relaxation processes are superimposed in the first few ps after excitation. In line with this, several suggestions have been put forward to explain the excitation wavelength dependence of the early absorbance difference spectra in WT RCs. These include multiphasic energy and electron transfer caused by incomplete nuclear relaxation on the time scale of energy and electron transfer (19–21). As yet, no clear-cut conclusion has been obtained as to the origin of this excitation wavelength dependence.

In this work we have performed pump-probe transient absorption measurements at 77 K on membrane-bound WT *R. sphaeroides* RCs, with selective excitation of different bacteriochlorin cofactors. Global analysis of datasets obtained with

The publication costs of this article were defrayed in part by page charge payment. This article must therefore be hereby marked “advertisement” in accordance with 18 U.S.C. §1734 solely to indicate this fact.

PNAS is available online at www.pnas.org.

This paper was submitted directly (Track II) to the *Proceedings* office. Abbreviations: Bchl, bacteriochlorophyll; P, primary donor of electrons; RC, reaction center; WT, wild type; SADS, species-associated difference spectrum; IRF, instrument response function.

§To whom reprint requests should be addressed. e-mail: rienk@nat.vu.nl.

different excitation wavelengths allowed us to distinguish energy transfer from the subsequent electron transfer process that leads to the formation of $P^+H_A^-$. After this deconvolution the spectral differences between the species-associated difference spectra (SADS) that lead to the formation of $P^+H_A^-$ can be interpreted in terms of a charge separation route in which mainly $P^+B_A^-$ is formed directly from B_A^* . A kinetic scheme is discussed that describes the kinetics and spectral changes of both the P and B excitation experiments.

MATERIALS AND METHODS

Sample Preparation. Experiments were performed on membrane-bound WT RCs from the antenna-deficient RCO2 strain of *R. sphaeroides* (22–25). Membranes in 10 mM Tris (pH 8.0) were mixed with glycerol in 3-mm cuvettes (60% vol/vol) and cooled to 77 K in an Oxford cryostat DN1704.

Time-Resolved Spectroscopy. Transient absorbance difference spectra were recorded by using a laser spectrometer as described in refs. 18, 22, and 23. The full width at half maximum of the instrument response function (IRF) was 350 fs. Data were collected in overlapping 130-nm wide wavelength windows centered at 800 nm and 890 or 900 nm. Typically 15% of the RCs were excited. In each wavelength window between one and four time series of spectra were included in the global analysis. In a typical time series approximately 90 spectra were collected at delay times between -0.3 ps and 150–300 ps. The delay time between the spectra varied between 40 fs and 40 ps with approximately 45 spectra being recorded in the first 5 ps.

Data Analysis. Global analysis was performed as described in ref. 18 with the addition that the wavelength dependence of time-zero caused by group velocity dispersion (GVD) was taken into account. To achieve this, the rise and decay of the optical Kerr signal in CS_2 measured over the different wavelength windows was analyzed with a third-order polynomial function to describe the variation of time zero of the IRF. The transient spectra (see Fig. 2) are the fitted spectra reconstructed from the smoothed average of the SADS estimated in the global analysis and corrected for GVD and IRF. In Fig. 4 raw measured spectra and kinetic traces are depicted, together with the result of the fit. Minor shifts were observed in the maximum of the bleaching of P between different experiments, which were not related to the excitation wavelength. The transient absorbance difference spectra were shifted by a maximum of 2 nm to overlay the P band bleaching signal in the $P^+Q_A^-$ and $P^+H_A^-$ difference spectra.

RESULTS

Transient Absorbance Difference Spectra. To investigate the dynamics of charge separation upon excitation of different bacteriochlorins, pump-probe experiments were performed at 77 K with selective excitation in the B and P Q_y absorbance bands (see Fig. 1). The low-energy exciton state of P (P_-) was excited at 880 nm, B_A was excited at 796 nm, and a combination of B_B and the high-energy exciton component of P (P_+) was excited at 818 nm (27). However, given the relatively broad excitation pulses and partially overlapping absorbance bands of B_A and B_B , and given the possibility that B_A and B_B might be excitonically mixed (28), excitation in the B band will be only partial selective. In Fig. 2 A–D, difference spectra obtained at 600 fs, 1 ps, 5 ps, and 200 ps after a 200-fs laser flash are presented for 880 and 796 nm excitation. Given that P^* -driven charge separation takes place with a lifetime of 1–2 ps at 77 K, the difference spectrum 5 ps after 880-nm excitation is that of $P^+H_A^-$ (Fig. 2C, dotted). This spectrum is characterized by bleaching of the H and P bands, at 750 nm and 890 nm respectively, and a strong electrochromic bandshift of the B band with an isosbestic point around 800 nm. The difference spectrum recorded 5 ps after 796-nm excitation (Fig. 2C, solid)

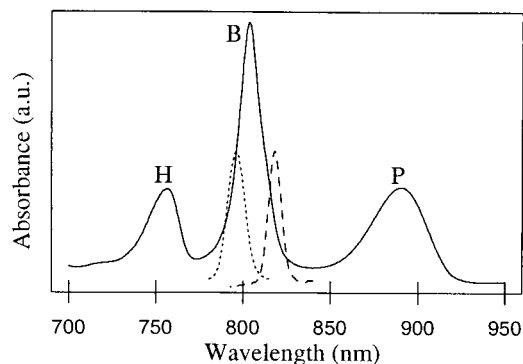


FIG. 1. 77 K absorption spectrum of RC-only membranes from *R. sphaeroides* strain RCO2. The profiles of the 796-nm and 818-nm excitation pulses used in this study are depicted by dashed and dotted lines, respectively.

is similar to the spectrum recorded 5 ps after 880-nm excitation. The difference spectra recorded at 200 ps, which can be attributed to the $P^+Q_A^-$ state, are also similar for both excitation wavelengths and show bleaching of P and electrochromic bandshifts over the B and H bands (Fig. 2D).

The difference spectrum recorded 600 fs after 880-nm excitation (Fig. 2A, dotted line) can be interpreted as mainly arising from P^* , although a small contribution from $P^+H_A^-$ is already present. In a RC in which all excitation energy of the monomeric Bchls is transferred to P in 100–200 fs, a difference spectrum recorded after 600 fs mainly would show the characteristics of P^* , irrespective of the excitation wavelength. Fig. 2A clearly demonstrates that this is not the case. The spectrum recorded 600 fs after 796-nm excitation (Fig. 2A, solid line) shows a strong bleach of the B band and somewhat less stimulated emission from P^* than is seen in the spectrum at 600 fs after 880-nm excitation (Fig. 2A, dotted line). After 1 ps, P^*

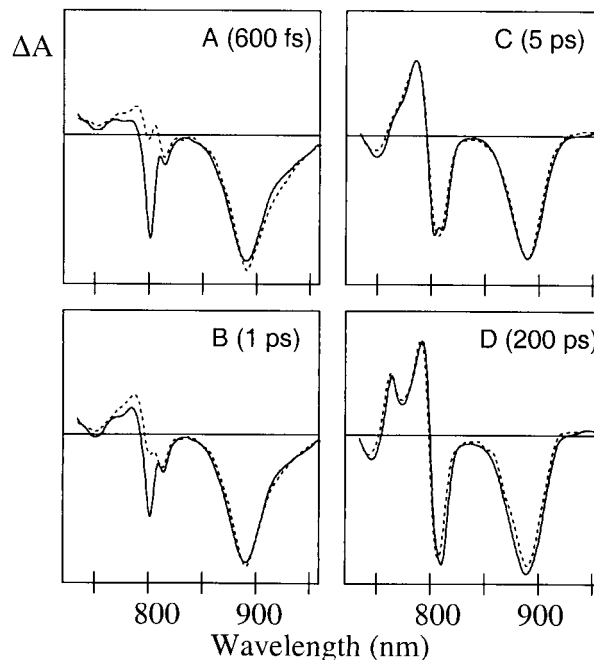


FIG. 2. Transient absorbance difference spectra obtained at 600 fs (A), 1 ps (B), 5 ps (C), and 200 ps (D) after a ~ 200 -fs excitation pulse centered at 796 nm (solid lines) and 880 nm (dotted lines). The spectra are reconstructed from the global analysis and are corrected for group velocity dispersion and IRF. The spectra were normalized to the maximum amplitude of the bleach of the P absorbance band at 5 ps (C).

has partially decayed to $P^+H_A^-$ and in accordance with this, the spectrum recorded 1 ps after 880-nm excitation shows a partial development of the electrochromic bandshift over the B absorbance band (Fig. 2B, dotted line). In comparison, the spectrum at 1 ps after 796-nm excitation displays a persistent bleach of the B band (Fig. 2B, solid line).

Global Analysis. To obtain the lifetimes associated with the spectral changes shown in Fig. 2, a global analysis of the datasets obtained after 880-, 818-, and 796-nm excitation was performed by using an irreversible sequential model (18). This model is close to a true physical model only for the 880-nm excitation experiment, because the first sub-ps process that follows excitation of B is probably a branched reaction (16, 17). This means that the SADS derived from the 880-nm excitation experiment are likely to represent true states, whereas for the experiments in which B was excited the SADS formed after the first sub-ps process should be viewed as representing a mixture of more than one true state (see *Discussion*).

Global analysis of the 880-nm excitation data shows that three kinetic components are necessary for a satisfactory fit (Fig. 3 A–C). The first SADS in Fig. 3A resembles the difference spectrum, which is formed directly after the 880-nm excitation pulse and represents P^* , with a bleach of the P band, a strong contribution caused by stimulated emission, and a sharp positive band at 806 nm. P^* decayed with a lifetime of 1.5 ps to $P^+H_A^-$, the SADS of which is shown in Fig. 3B. An additional kinetic component for the two-step electron transfer mechanism $P^* \rightarrow P^+B_A^- \rightarrow P^+H_A^-$ was difficult to resolve. This is probably related to the very low transient population of the intermediate $P^+B_A^-$ (see below) and the fact that we have not measured accurate kinetic traces around the isosbestic point of the $P^+H_A^-$ bandshift or in the 1,020-nm region, which previously has resulted in the resolution of this kinetic component (7–10). The transition from $P^+H_A^-$ to $P^+Q_A^-$ was associated with a lifetime of 80 ps, and the SADS of $P^+Q_A^-$ shows the development of the bandshift over the H band and a red-shift of the isosbestic point of the bandshift over the B band (Fig. 3C).

For the B excitation experiments, a restriction was made to the fit such that the first SADS, which resembles the difference spectrum of B^* , did not have a contribution above 840 nm, which resulted in a more precise determination of time zero in the P absorbance region. This restriction did not significantly increase the rms error of the residuals, nor did it affect the

spectral shape and lifetime of the other SADS. When parameters in the fitting procedure were varied, such as by using a fixed or fitted IRF, or including amplitude in the first SADS above 840 nm, the fitted lifetime of the first SADS after 796-nm excitation varied between 160 and 200 fs and between 60 and 120 fs for the first SADS in the 818-nm excitation experiment.

Global analysis of the data recorded after 796-nm excitation revealed four lifetimes of 180 fs, 1.7 ps, 70 ps, and a fixed infinite lifetime for the $P^+Q_A^-$ spectrum (Fig. 3 D–G). The first SADS resembles the spectrum of B^* , showing a strong bleach at 801 nm (Fig. 3D). As the 796-nm excitation pulse preferentially excites B_A , the bleach associated with B^* does not cover the whole of the B absorbance band. In particular, the shoulder at 811 nm in the absorbance spectrum, which is caused by absorbance of B_B and P_+ (27) is not completely bleached. B^* decayed with a lifetime of 180 fs, partly through energy transfer to P, as can be seen from the appearance of a bleach of the P band and stimulated emission in the second SADS (Fig. 3E). However, this second SADS is very different from the SADS attributed to P^* in the 880-nm excitation experiment (Fig. 3A). Comparison of the two spectra in the B absorbance region shows that the SADS formed from B^* exhibits a large bleach at 801 nm in addition to increased absorbance attributable to P^* , which is seen as a positive feature on the red side of the 801-nm bleach. The third SADS has the characteristics of the difference spectrum of $P^+H_A^-$ (Fig. 3F), and is similar to the SADS obtained for $P^+H_A^-$ after 880-nm excitation (Fig. 3B). $P^+H_A^-$ decays to $P^+Q_A^-$ (Fig. 3G) with a lifetime of 70 ps, similar to the 80-ps process after 880-nm excitation.

By using 818 nm light, mainly B_B and P_+ , together with some B_A , are excited (27). After an initial ~ 100 -fs decay of B^* (Fig. 3H), a state was formed with a SADS (Fig. 3I) that could be described as a combination of the P^* spectrum obtained after 880-nm excitation, and the spectrum obtained after relaxation of B^* by using 796-nm excitation (see Fig. 5C). A lifetime of 2 ps describes the evolution of this SADS to $P^+H_A^-$ (Fig. 3J), which in turn decayed to $P^+Q_A^-$ in 77 ps (Fig. 3K).

To show the success of the global analysis fit, Fig. 4 A–C shows kinetic traces for the 796-nm excitation experiments (which are sections through the transient absorbance difference spectra at the selected wavelengths) together with the results of the fit. Fig. 4 D–F shows typical uncorrected transient

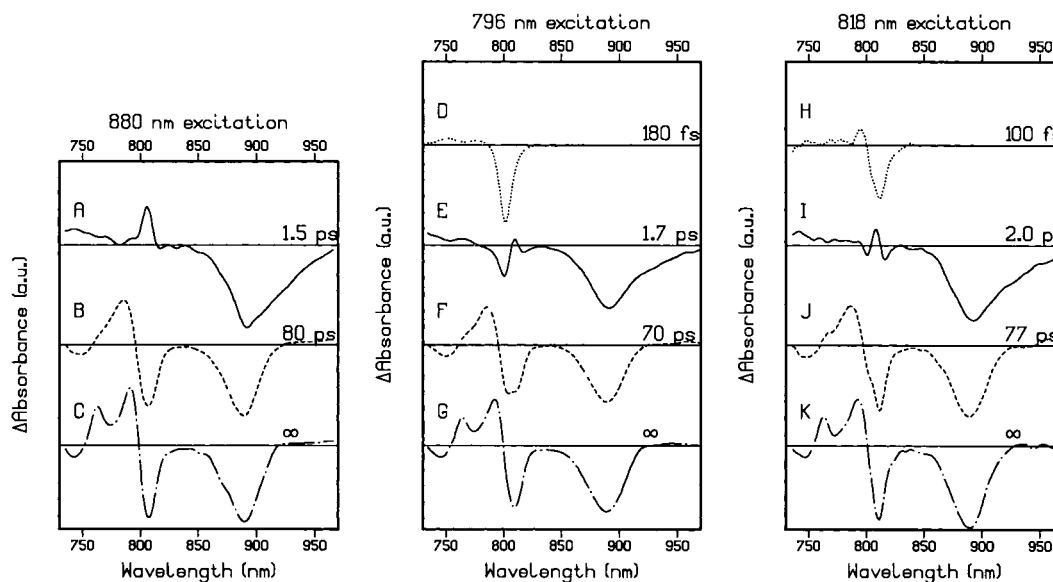


FIG. 3. SADS and associated lifetimes derived from a global analysis of the transient absorbance difference spectra obtained after 880-nm (A–C), 796-nm (D–G), and 818-nm (H–K) excitation. For the purpose of comparison, spectra D and H have been multiplied by a factor of 0.2.

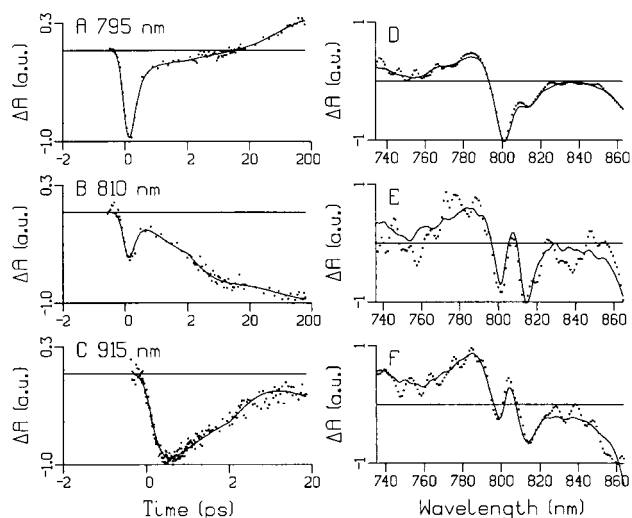


FIG. 4. (A–C) Kinetic absorbance difference traces at 795, 810, and 915 nm obtained after a ~ 200 -fs excitation pulse at 796 nm. The time axes are linear between -2 and 2 ps and logarithmic between 2 and 200 ps. The global analysis fit is depicted with the solid line. (D–F) Typical uncorrected transient absorbance difference spectra (points) recorded at 950, 750, and 700 fs after 796-, 818-, and 880-nm excitation, respectively, together with the result of the global analysis fit (solid line). The maximal ΔOD is 0.04, 0.012, and 0.02 OD for spectrum D–F, respectively.

absorbance difference spectra at 950, 750, and 700 fs after 796-, 818-, and 880-nm excitation, respectively, together with the results of the fit. The residuals of the fit show a random character in time and the rms error of the fit is 2–3 mOD compared with a maximal P bleach of typically 60 mOD.

To summarize, excitation of B at 796 nm and 818 nm results in a ~ 180 and ~ 100 fs relaxation of B^* , respectively. After the decay of B^* , the state $P^+H_A^-$ is formed in 1.5–2 ps, a lifetime similar to that found when P is excited directly. The subsequent electron transfer from $P^+H_A^-$ to $P^+Q_A^-$ takes place in 70–80 ps. However, the spectral differences between the SADS of the states that precede the formation of $P^+H_A^-$ show that after excitation of B at 796 nm, a state is formed directly from B^* in which B absorbance is strongly bleached, in a process operating in parallel with energy transfer to P.

DISCUSSION

Excitation Wavelength Dependence Before $P^+H_A^-$. Fig. 5A shows an overlay of the SADS of the states from which $P^+H_A^-$ is formed in 1.5 ps and 1.7 ps after 880-nm and 796-nm excitation, respectively (i.e. Fig. 3A and E). The spectra in Fig. 5A were scaled to the maximum amplitude of the bleach of the P band in the $P^+H_A^-$ SADS from each experiment (Fig. 3B and F). In the B absorbance region, the 880-nm excitation SADS shows a sharp absorbance increase at 806 nm (Fig. 5A, dotted line), whereas the 796-nm excitation SADS is dominated by a bleach of the ground state absorbance of B at 801 nm (Fig. 5A, solid line). From this comparison it is also clear that the 796-nm excitation SADS exhibits less stimulated emission from P^* than the 880-nm excitation SADS. The bleach of B and the diminished amount of P^* -stimulated emission seen in the SADS from the 796-nm experiment can be accounted for by a contribution of the state $P^+B_A^-$ to this spectrum. Alternatively, we could consider slow relaxations of B^* to explain the observed spectral changes. However, in view of the following arguments we consider this to be unlikely. In the YM210W mutant excitation of B at 799 nm results in alternative charge separation plus energy transfer to P. The B^* state fully decays with a ~ 200 -fs lifetime and a priori there is

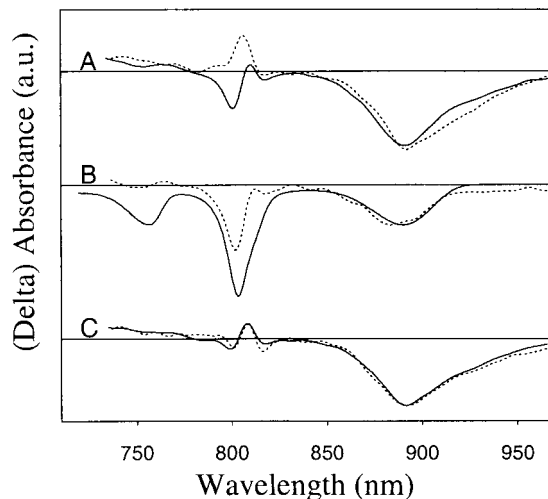


FIG. 5. (A) Overlay of the SADS from Fig. 3A (dotted line) and 3E (solid line). The spectra were normalized on the P bleaching in the relevant $P^+H_A^-$ SADS (Fig. 3B and F, respectively). (B) Comparison of the difference between the 796-nm excitation SADS of A and 60% of the 880-nm excitation SADS of A (dotted line) with the minus ground state absorbance spectrum (solid line). (C) Comparison of the sum (equal contributions) of the 880- and 796-nm excitation SADS from A (solid line) with the 818-nm excitation SADS from Fig. 3I (dotted line).

no reason this would be different for the WT RC. In fact, because the absorption spectra of the YM210W mutant and the WT RC are very similar (22) and, a 2.7-Å resolution x-ray structure of the YM210W does not show any changes that could have a significant effect on the rate of energy transfer from B^* to P, the energy transfer lifetimes are expected to be very similar (K. E. McAuley-Hecht, P. K. Fyfe, N. W. Isaacs, R. J. Cogdell, and M.R.J., unpublished results). A slow B^* decay can not explain the missing stimulated emission compared to the amount of P groundstate bleach observed by us and others (19–21). That $P^+B_A^-$ is a likely candidate is further illustrated in Fig. 5B, where 60% of the P^* SADS obtained from the 880-nm excitation experiment (Fig. 5A, dotted line) is subtracted from the 1.7-ps, 796-nm excitation SADS (Fig. 5A, solid line) and the remaining spectrum is compared with the inverse ground state absorbance spectrum normalized on the P absorbance bleach. This double difference spectrum shows a strong bleach on the blue side of the B absorbance band and bleach of P groundstate absorbance, thus resembling the $P^+B_A^-$ difference spectrum as reported in the literature (7, 9–11). This finding indicates that the SADS obtained after 796-nm excitation represents a mixture of about equal ($\sim 60:40\%$) contribution of P^* and $P^+B_A^-$. In contrast to our experiments on the YM210W (18), YM210L (17), and HM202L heterodimer RCs (M.E.v.B., I.H.M.v.S., E. Katilius, F.v.M., M.R.J. & R.v.G., unpublished results) we do not have an indication that $B_A^+H_A^-$ is formed, i.e. no significant bleach of H is observed in the 1.7-ps, 796-nm excitation SADS, and no increase of the amount of P groundstate absorbance bleach at later times is resolved that would indicate the reaction $B_A^+H_A^- \rightarrow P^+H_A^-$.

The SADS of the state before the formation of $P^+H_A^-$ after 818-nm excitation can be described by the sum of the equivalent SADS from the 796-nm and 880-nm excitation experiments (see Fig. 5C), which can be interpreted in terms of excitation of B_B and P_+ by 818-nm light yielding a P^* state that was similar to that created on direct excitation of P, together with some excitation of B_A by the 818-nm excitation pulse (see Fig. 1). This finding strongly suggests that it is the active branch monomeric Bchl that is involved in the alternative electron transfer pathway, which is in line with the fluores-

cence excitation spectrum of the YM210W mutant (16) and recent photon echo experiments (26).

Kinetic Modeling. For all three excitation wavelengths used in this study, we find that the formation of $P^+H_A^-$ is associated with a lifetime of between 1.5 and 2 ps. However, the spectral changes associated with these lifetimes are very different after excitation of either B at 796 nm or P at 880 nm (Figs. 2 and 3). We attribute this effect to evolution of part of B_A^* into the charge-separated state $P^+B_A^-$. At first sight it is surprising that although clear spectral contributions for the presence of $P^+B_A^-$ are observed, no separate kinetic component for this intermediate is resolved. However, this can be understood on the basis of the kinetic simulation depicted in Fig. 6. The numbers chosen for the lifetimes in this simulation reflect the fitted lifetimes and spectral information in the SADS but should not be considered as definitive numbers, because there is some experimental variation between the fitted lifetimes that describe the formation of $P^+H_A^-$ (1.5–2 ps) for the different excitation wavelengths. Also the transition $P^+B_A^- \rightarrow P^+H_A^-$ has not been resolved kinetically in this P excitation experiment. In this kinetic scheme it is assumed for the reactions $P^* \rightarrow P^+B_A^- \rightarrow P^+H_A^-$ that the formation of $P^+B_A^-$ from P^* takes place with a lifetime of 1.7 ps and that the decay from $P^+B_A^-$ to $P^+H_A^-$ is two times faster, i.e. 0.85 ps. Upon excitation of P, this results in a low population of $P^+B_A^-$, as can be seen in the concentration profile in Fig. 6A. As a consequence, the spectral changes after P excitation are dominated by the decay of P^* and the ingrowth of $P^+H_A^-$. In Fig. 6B, equal amounts of $P^+B_A^-$ and P^* are formed from B^* with a 180-fs lifetime. We can not decide whether the 180-fs lifetime for B^* reflects the sum of two competitive decays of 360 fs each or represents a parallel decay in two fractions of RCs; one in which B_B^* transfers energy to P and a second in which direct charge separation is driven by B_A^* . Most likely, a combination of these processes occurs. In Fig. 6B the situation with the competitive decay is depicted, but we note that the two 360-fs lifetimes are just effective lifetimes to simulate the

180-fs decay and the 50-50% branching between both pathways. The remaining part of the kinetic scheme in Fig. 6B is identical to Fig. 6A. Surprisingly, according to this kinetic scheme the concentration profiles of $P^+B_A^-$ and P^* are identical, (the crosses and solid line in Fig. 6B, which depict the concentration profile of $P^+B_A^-$ and P^* , respectively, show identical kinetics) and both states are being formed with an observable lifetime of 180 fs and decay with an observable lifetime of 1.7 ps. For $P^+B_A^-$ the 1.7-ps observable lifetime is the result of the assumed 50/50% branching from B^* into $P^+B_A^-$ and P^* and the difference between the $1/0.85\text{-ps}^{-1}$ decay of $P^+B_A^-$ and the simultaneous $1/1.7\text{-ps}^{-1}$ ingrowth of $P^+B_A^-$ formed from P^* . Of course, if the ratio of the rate constants for the transitions $P^* \rightarrow P^+B_A^-$ and $P^+B_A^- \rightarrow P^+H_A^-$ were to be different from 1:2, or if the initial populations of P^* and $P^+B_A^-$ formed from B^* were not equal, this would result in different profiles for P^* and $P^+B_A^-$. However, small changes in these parameters still would lead to very similar concentration profiles for $P^+B_A^-$ and P^* and would make them indistinguishable in practice. This kinetic scheme thus gives a good description of the results of the 796-nm excitation experiment, where $P^+B_A^-$ and P^* are formed from B^* in approximately equal amounts and in which a decay of 1.7 ps with spectral contributions from both $P^+B_A^-$ and P^* describes the formation of $P^+H_A^-$.

From comparison of the B^* lifetime found in the 796-nm and 818-nm excitation experiment, it appears that energy transfer is faster upon excitation at the red side of the B absorbance band than upon the blue side, as has been described previously (20, 26). This could be related to fast internal conversion of P_+^* to P_-^* and/or to faster energy transfer from the more red emitting B_B^* to P_+/P_- than from B_A^* to P_+/P_- .

The Significance of Multiple Strategies for Achieving Charge Separation in the RC. In WT strains of *R. sphaeroides* almost all excitation energy is harvested by the antenna pigments and funnelled to the RC Bchl dimer P (29). As a result, except for the rare occasions when $B_{A,B}$ or $H_{A,B}$ of the RC directly absorbs a photon, the excited state formed in the RC will be P^* , and the P^* -driven route for charge separation will dominate.

The alternative pathways that exist in the bacterial RC may have significant ramifications for the RCs from higher plants, where the mechanism of light-driven charge separation is less well understood. There is considerable debate concerning the nature of the excited state that drives charge separation in the photosystem II (PSII) RC. In dramatic contrast to the absorption spectrum of the bacterial RC, where the transition of P is clearly separated from the B and H contributions, all the chlorins in the PSII RC absorb in a narrow spectral region between 670 and 680 nm. As a consequence the interaction between the pigments in the PSII RC can not be larger than 100 cm^{-1} , which is of the same order of magnitude as the intrinsic disorder (30, 31). A straightforward calculation (31) then demonstrates that each excited state of the PSII RC is shared by on average three chlorins and in general is not specifically localized on the special pair. Polarized transient absorption (32) and energy selective fluorescence experiments (33) recently have been interpreted in terms of this weakly coupled multimer model for the PSII RC. From temperature dependent transient absorption experiments it was furthermore concluded (34) that charge separation in the PSII RC occurred via the sub-ps formation of a charge-separated state from one of the excited states. Our experiments are fully consistent with this hypothesis and show that the excited state of a special pair is not an absolute prerequisite for ultrafast electron transfer. In fact, the fast electron transfer may be equally well driven by an excited state localized (in part) on the monomeric chlorophyll in the active branch. In addition, our data shows that the (B)Chls that participate in the excited state that drives charge separation are not necessarily the same as

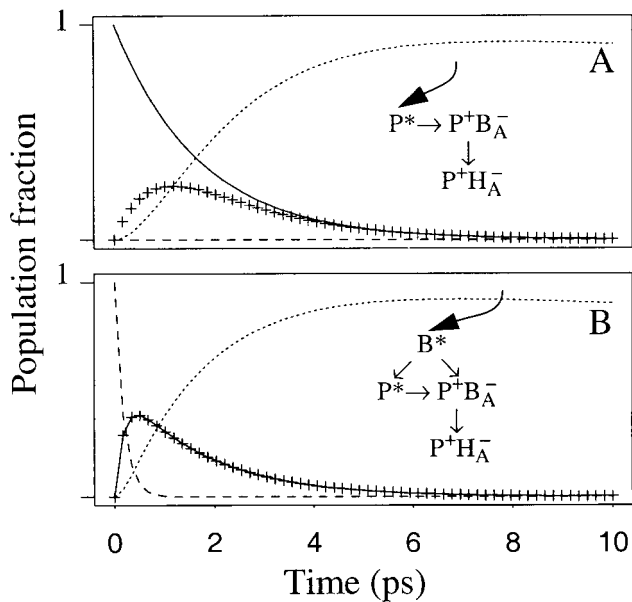


FIG. 6. Kinetic scheme to describe the experiments in which P (880 nm) and B (796 nm) are excited. The concentration profiles of B^* (dashed line), P^* (solid line), $P^+B_A^-$ (crosses), and $P^+H_A^-$ (dotted line) were calculated according to the depicted kinetic scheme for P (A) and B (B) excitation by using lifetimes of 360 fs for $B^* \rightarrow P^+B_A^-$, 360 fs for $B^* \rightarrow P^*$, 1.7 ps for $P^* \rightarrow P^+B_A^-$, 0.85 ps for $P^+B_A^- \rightarrow P^+H_A^-$, and 80 ps for the state $P^+H_A^-$. At time zero the population was considered to be 100% B^* and 100% P^* for B and P excitation, respectively.

those that carry the cation that is the stable product of charge separation, as in the alternative pathway discussed above B_A^* gives rise to P^+ .

Mechanism of Electron Transfer in Bacterial RCs. The ultrafast electron transfer events with lifetimes on the order of hundreds of fs probably can not be described within the framework of nonadiabatic electron transfer theory (35). Analysis of the free energy dependence of the primary electron transfer step $P^* \rightarrow P^+B_A^-/P^+H_A^-$ using mutants with different P/P^+ redox potentials have placed the primary electron transfer step in WT RCs near to the top of the Marcus parabola (23, 36), which means that this electron transfer step is energetically optimized and that the rate of this process is limited by the electronic coupling between the donor and acceptor states. The extra energy present in the excited state of B_A is thus not sufficient to explain why the formation of $P^+B_A^-$ from B_A^* takes place with a lifetime of about 400 fs or shorter. A difference in electronic coupling could explain the different rates for the formation of $P^+B_A^-$ from B_A^* and P^* . This is supported by calculations based on the RC structure, which indicate that the coupling between the lowest unoccupied molecular orbital (LUMO) of P and the LUMO of B, defining the reaction rate for $P^* \rightarrow P^+B_A^-$, is significantly weaker than the coupling between the highest occupied molecular orbital (HOMO) of B and the HOMO of P for the reaction $B_A^* \rightarrow P^+B_A^-$, i.e. about 10 cm^{-1} versus 50 cm^{-1} . Based solely on these numbers the formation of $P^+B_A^-$ would be 20–30 times faster from B_A^* than from P^* (S. F. Fischer and P. O. J. Scherer, personal communication), which would be faster than the observed 150- to 400-fs lifetime. This could mean that the charge separation driven by B_A^* is limited by nuclear relaxation. The possibility of an adiabatic electron transfer mechanism for the primary processes also has been suggested previously on the basis of transient absorbance, hole burning, and photon echo experiments (19, 20, 26, 37).

To close, it appears that RCs as a group possess a rich variety of paths along which they can perform charge separation, the path using the special pair being just one of them. In fact, from these results it must be obvious that the special pair is most likely not there for the greatest possible rate for charge separation; it simply can go much faster. In this respect it should be noted that a sub-ps lifetime for charge separation is not restricted to B_A^* , but that a mutant RC of *Rps. viridis* has been described in which P^* performs charge separation with a 250-fs lifetime at cryogenic temperature (7). Most likely, the need to have a state resonant with the LH1 antenna required the bacterial RC to have a state at similar energy and the special pair was one way to achieve this. In plants, this requirement is relaxed, and possibly their reaction centers exploit all possible routes for ultrafast electron transfer.

M.R.J. acknowledges support from the Biotechnology and Biological Sciences Research Council. M.E.v.B. and F.v.M. are supported by the Dutch Foundation for Fundamental Research (NWO) through the foundation for Life and Earth Sciences (ALW).

- Allen, J. P., Feher, G., Yeates, Y. O., Komiya, H. & Rees, D. C. (1987) *Proc. Natl. Acad. Sci. USA* **84**, 5730–5734.
- Ermler, U., Fritsch, G., Buchanan, S. K. & Michel, H. (1994) *Structure* **2**, 925–936.
- Parson, W. W. (1996) in *Protein Electron Transfer*, ed. Bendall, D. S., (Bios Scientific, Oxford), pp. 125–148.
- Fleming, G. R. & van Grondelle, R. (1994) *Phys. Today* **47**, 48–55.
- Woodbury, N. W., Becker, M., Middendorf, D. & Parson, W. W. (1985) *Biochemistry* **24**, 7516–7521.
- Fleming, G. R., Martin, J. L. & Breton, J. (1988) *Nature (London)* **333**, 190–192.
- Zinth, W., Huppmann, P., Arlt, T. & Wachtveitl, J. (1998) *Phil. Trans. R. Soc. London Ser. A* **356**, 465–475.
- Lauterwasser, C., Finkele, U., Scheer, H. & Zinth, W. (1991) *Chem. Phys. Lett.* **183**, 471–477.
- Holzwarth, A. R. & Müller, M. G. (1996) *Biochemistry* **35**, 11820–11831.
- van Stokkum, I. H. M., Beekman, L. M. P., Jones, M. R., van Brederode, M. E. & van Grondelle, R. (1997) *Biochemistry* **36**, 11360–11368.
- Kennis, J. T. M., Shkuropatov, A. Ya., van Stokkum, I. H. M., Gast, P., Hoff, A. J., Shuvalov, V. A. & Aartsma, T. J. (1997) *Biochemistry* **36**, 16231–16238.
- Stanley, R. J., King, B. & Boxer, S. G. (1996) *J. Phys. Chem.* **100**, 12052–12059.
- Jonas, D. M., Lang, M. J., Nagasawa, Y., Joo, Y. & Fleming, G. R. (1996) *J. Phys. Chem.* **100**, 12660–12673.
- Wynne, K., Haran, G., Reid, G. D., Moser, C. C., Dutton, P. L. & Hochstrasser, R. M. (1996) *J. Phys. Chem.* **100**, 5140–5148.
- Haran, G., Wynne, K., Moser, C. C., Dutton, P. L. & Hochstrasser, R. M. (1996) *J. Phys. Chem.* **100**, 5562–5569.
- Van Brederode, M. E., Jones, M. R. & van Grondelle, R. (1997) *Chem. Phys. Lett.* **268**, 143–149.
- Van Brederode, M. E., Ridge, J. P., van Stokkum, I. H. M., van Mourik, F., Jones, M. R. & van Grondelle, R. (1998) *Photosynth. Res.* **55**, 141–146.
- Van Brederode, M. E., Jones, M. R., van Mourik, F., van Stokkum, I. H. M. & van Grondelle, R. (1997) *Biochemistry* **36**, 6855–6861.
- Lin, S., Taguchi, A. K. W. & Woodbury, N. W. (1996) *J. Phys. Chem.* **100**, 17067–17078.
- Vos, M. H., Breton, J. & Martin, J.-L. (1997) *J. Phys. Chem.* **101**, 9820–9832.
- Lin, S., Jackson, J., Taguchi, A. K. W. & Woodbury, N. W. (1998) *J. Phys. Chem.* **102**, 4016–4022.
- Beekman, L. M. P., Visschers, R. W., Monshouwer, R., Heer-Dawson, M., Mattioli, T. A., McGlynn, P., Hunter, C. N., Robert, B., van Stokkum, I. H. M., van Grondelle, R. & Jones, M. R. (1995) *Biochemistry* **34**, 14712–14721.
- Beekman, L. M. P., van Stokkum, I. H. M., Monshouwer, R., Rijnders, A. J., McGlynn, P., Visschers, R. W., Jones, M. R. & van Grondelle, R. (1996) *J. Phys. Chem.* **100**, 7256–7268.
- Jones, M. R., Visschers, R. W., van Grondelle, R. & Hunter, C. N. (1992) *Biochemistry* **31**, 4458–4465.
- Jones, M. R., Heer Dawson, M., Mattioli, T. A., Hunter, C. N. & Robert, B. (1994) *FEBS Lett.* **339**, 18–24.
- Groot, M.-L., Yu, J.-Y., Agarwal, R., Norris, J. R. & Fleming, G. R. (1998) *J. Phys. Chem.* **102**, 5923–5931.
- Breton, J., Bylina, E. J. & Youvan, C. Y. (1989) *Biochemistry* **28**, 6423–6430.
- Reddy, N. R. S., Kolaczowski, S. V. & Small, G. J. (1993) *J. Phys. Chem.* **97**, 6934–6940.
- Van Grondelle, R., Dekker, J. P., Gillbro, T. & Sundström, V. (1994) *Biochim. Biophys. Acta* **1187**, 1–65.
- Kwa, S. L. S., Eijkelhoff, C., van Grondelle, R. & Dekker, J. P. (1994) *J. Phys. Chem.* **98**, 7702–7711.
- Durrant, J. R., Klug, D. R., Kwa, S. L. S., van Grondelle, R., Porter, G. & Dekker, J. P. (1995) *Proc. Natl. Acad. Sci. USA* **92**, 4798–4804.
- Merry, S. A. P., Kumazaki, S., Tachibana, Y., Joseph, D. M., Porter, G., Yoshihara, K., Barber, J., Durrant, J. R. & Klug, D. R. (1996) *J. Phys. Chem.* **100**, 10469–10478.
- Peterman, E. J. G., van Amerongen, H., van Grondelle, R. & Dekker, J. P. (1998) *Proc. Natl. Acad. Sci. USA* **95**, 6128–6133.
- Groot, M.-L., van Mourik, F., Eijkelhoff, C., van Stokkum, I. H. M., Dekker, J. P. & van Grondelle, R. (1997) *Proc. Natl. Acad. Sci. USA* **94**, 4389–4394.
- Marcus, R. A. & Sutin, N. (1985) *Biochim. Biophys. Acta* **811**, 265–322.
- Jia, Y., DiMagno, T. J., Chan, C.-K., Wang, Z., Du, M., Hanson, D. K., Schiffer, M., Norris, J. R. & Fleming, G. R. (1993) *J. Phys. Chem.* **97**, 13180–13191.
- Small, G. J. (1995) *Chem. Phys.* **197**, 239–257.